Direct numerical simulation of fluid–acoustic interactions in a recorder with tone holes

Hiroshi Yokoyama,[1,a)] Akira Miki,[2] Hirofumi Onitsuka,[2] and Akiyoshi Iida[1]
[1]*Department of Mechanical Engineering, Toyohashi University of Technology, Aichi 441-8580, Japan*
[2]*Research & Development Division, Yamaha Corporation, Shizuoka 438-0192, Japan*

(Received 13 February 2015; revised 30 June 2015; accepted 2 July 2015; published online 17 August 2015)

To clarify fluid–acoustic interactions in an actual recorder with opened and closed tone holes, flow and acoustic fields were directly numerically simulated on the basis of the compressible Navier–Stokes equations. To validate the simulation accuracy, the flow field around the windway and sound pressure above the window were measured. The predicted acoustic fields clarify changes of the positions of pressure nodes and anti-nodes in accordance with the state of the tone holes and the Mach number of the jet velocity. The fundamental mechanism of the self-sustained oscillations in a three-dimensional actual recorder is visualized by the predicted acoustic and flow fields. This result is also consistent with the relationship between the jet behaviors and pressure fluctuations based on the jet-drive model. Moreover, the effects of the fine vortices in the jet, which appear at the high Mach number of jet velocity of 0.099, on the sound are discussed. The time difference between the generation of the disturbances and the most intense deflection of the jet is identified and compared with the time delay of acoustic reflection around the window.
 [http://dx.doi.org/10.1121/1.4926902]

[AH] Pages: 858–873

I. INTRODUCTION

Flue instruments, such as flutes, bamboo flutes, and recorders, consist of an edge ("labium") with which an air jet collides and a resonator (pipe). In the oscillations in flue instruments, the feedback loop is formed.[1] The vorticity perturbations are induced at the flue exit due to acoustic particle velocity, which are amplified into jet oscillations, and the acoustic radiation occurs by the interaction of the jet oscillations and the edge. This acoustic radiation drives the acoustic resonance in the resonator.[1]

Since the pioneering works of Helmholtz[2] and Rayleigh,[3] many researchers have investigated the self-sustained oscillations of flow and sound in flue instruments. Helmholtz proposed a "volume-flow model" to describe the mechanism that supplies the acoustic power in the resonator from oscillations of the air jet. In this model, the deflection of the jet along the window (mouth) changes the flow rate of air into the resonator, thereby inducing compression and expansion in the resonator. Meanwhile, Rayleigh[3] mentions that the volume injection below the edge suggested by Helmholtz[2] would be quite inefficient because the injection point is close to a pressure node. Rayleigh proposed a "momentum-transfer model,"[3] in which the acceleration of the air flow by the jet increases the pressure, and thus the compression, in the resonator. Coltman[4] proposed a jet-drive model, where the role of the edge is a partitioning agent which determines the region into which air from the jet flows and complementary (dipolar) flow sources placed on each side of the edge due to the jet oscillations induce pressure difference across the window. This model was further developed by Verge *et al.*[5–7] Fabre and Hirschberg,[8] Meissner,[9] and Dequand *et al.*,[10] where a dipolar sound source can be represented as a fluctuating pressure discontinuity across the window in the framework of a lumped element model. Coltman[11] experimentally confirmed the superiority of the jet-drive model in comparison with momentum-transfer model.[3]

By generalization of the theory of vortex sound by Powell,[12] Howe[13] discussed the acoustic radiation due to vortex shedding at the edge. Meanwhile, by visualizing the jet oscillations, Fabre *et al.*[14] argued that the vortex shedding at the edge dissipates sound at the fundamental frequency rather than produces sound as suggested by Howe[13] because the large amplitude of the jet oscillations at the first oscillating mode and the limited width of the jet make Howe's model[13] inefficient. Fabre *et al.*[14] also insisted that the vortex shedding at the edge affects the distributions of higher harmonics. Using a horn-loudspeaker system and particle-image velocimetry (PIV), Yoshikawa *et al.*[15] measured jet velocity and acoustic cross-flow velocity fields separately. As a result, they demonstrated that acoustic power is dominantly generated by the flow-acoustic interaction near the edge.

Regarding the generation and amplification of jet oscillations, Rayleigh[3] and Cremer and Ising[16] focused on instability of the jet, which amplifies the jet oscillations in the downstream. Fletcher[17] expressed the displacement of the jet along the window with time by using a physical-intuition model—called a "negative displacement model"—consisting of the component of acoustic mass flow and the component convected and amplified in the downstream. In this model, the latter component is a negative value in relation to the former component. Moreover, Yoshikawa and Saneyoshi[18] proposed a pressure-gradient model, in which

[a)]Electronic mail: h-yokoyama@me.tut.ac.jp

the pressure difference between the upper and lower sides of the jet causes the jet oscillations. However, the intrinsic instability of the jet, which was described by Fletcher[17] and Fabre and Hirschberg,[8] was ignored in this model. By measuring the displacement of the jet and acoustic mass flow, Coltman[4,19] proposed that acoustic particle velocity at the window is the source of the jet oscillations. However, the above-mentioned studies have only discussed simplified models, and the mechanism of the fluid−acoustic interactions in a three-dimensional actual flue instrument has not been clarified.

To predict the resonant frequency, the open end corrections for the resonator exit and tone holes need to be clarified. Benade[20] estimated the end corrections for tone holes on the basis of the measured resonant frequency. Using Green-function expansions, Keefe[21] theoretically investigated the effects of a tone hole with a chimney on the acoustic field in a cylindrical bore. Using numerical simulations based on boundary element method (BEM) and finite difference method (FDM), Dalmont *et al.*[22] predicted the open end corrections of cylindrical tubes with various shapes. However, the effects of tone holes and jet velocity on the standing waves during the self-sustained oscillations in an actual recorder have not been clarified.

Segoufin *et al.*[23] experimentally investigated the effects of windway (channel) length and window geometry on the sound of a simplified flue instrument, and they clarified that adding chamfers to a long windway greatly gives the instrumentalist a wider playing range of jet velocity on a given mode of the resonator. Auvray *et al.*[24] clarified the dependency of the oscillating frequency on the jet velocity using a linear acoustic theory including the change of regime. Using direct numerical simulations based on the three-dimensional Navier-Stokes equations under the assumption of adiabatic conditions, Giordano[25] simulated the effects of the chamfers of the windway exit and the position of the edge (with reference to the windway) on the tonal sound. However, the model was made by extruding a two-dimensional cross section like that of a recorder, and the three-dimensionality of shape of an actual instrument was not incorporated in the model. Although this simulation predicted that the fundamental frequency was increased at higher jet velocity[25] and that result was confirmed by Bak,[26] the quantitative relationship between the fluid–acoustic interactions and the variation of frequency has not been clarified. Using compressible large-eddy simulation (LES), Miyamoto *et al.*[27] compared the flow and acoustic fields in a two-dimensional model with those in the quasi-two-dimensional model (three-dimensional model) consisting of a volume between two parallel non-slip walls. As a result, it was clarified that the jet is more unstable due to the long-life vortex tubes existing in the two-dimensional model compared with that in the three-dimensional model. However, the shape of the cross section is rectangular and the resonator has a closed end, which are different from those of an actual instrument.

In the present investigation, to clarify the fluid–acoustic interactions occurring around an actual recorder with opened and closed tone holes, direct numerical simulations (based on the compressible Navier-Stokes equations) using models

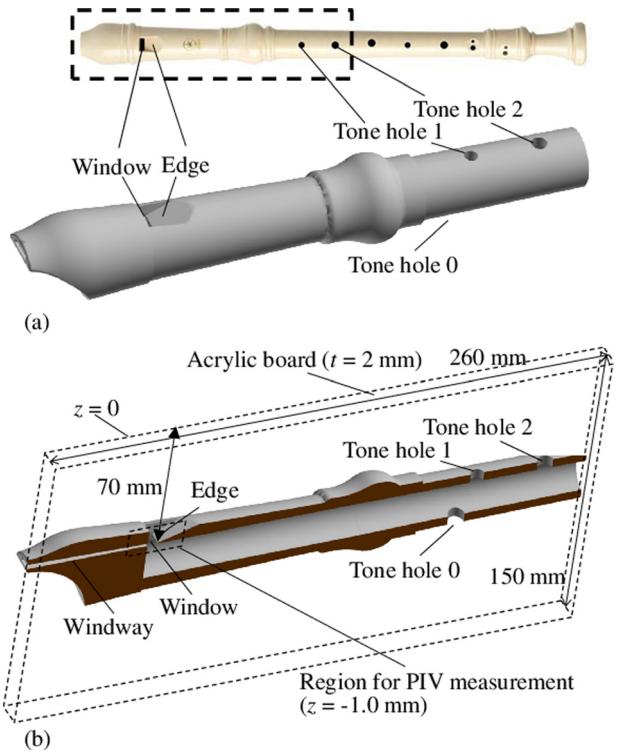

FIG. 1. (Color online) Computational and experimental models of recorder (YRA-28BIII): (a) full model and (b) half model.

of an actual recorder (YRA-28BIII), as shown in Fig. 1, were performed. Also, to validate the computational accuracy of the simulation, the velocity field and sound-pressure level were measured by PIV and microphone, respectively.

In Sec. IV A, based on the predicted flow and acoustic fields, the feedback-loop mechanism of the self-sustained oscillations (including generation of acoustic power and jet oscillations due to acoustic feedback) is clarified. In Sec. IV B, the effects of the state of tone holes and the jet velocity

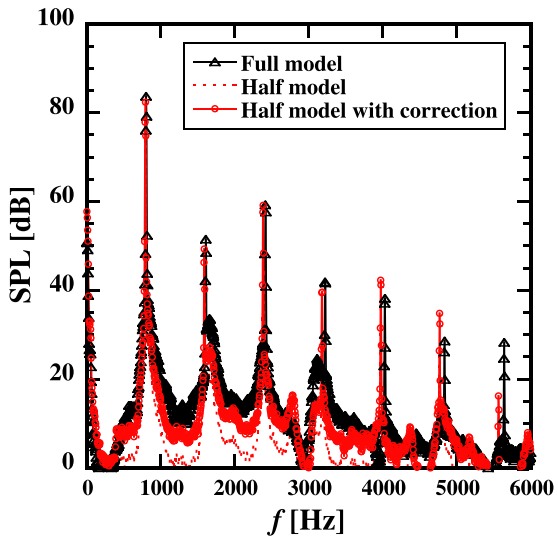

FIG. 2. (Color online) Measured sound spectra in case of all holes open at $M = 0.033$ at $x = 0$, $y = 500$ mm, and $z = 0$ for half and full models, where the corrected spectrum for half model is also shown.

on the mechanism proposed in Sec. IV A are discussed. In Sec. IV C, the effects of the state of tone holes and the jet velocity on the standing waves in the resonator are discussed.

II. METHODOLOGIES

A. Flow conditions

The flow and acoustic fields around a recorder were investigated by using a short recorder with three tone holes (see Fig. 1), namely, an actual recorder (YRA-28BIII) cut short after the third hole, as a model (called a "full model" hereafter). The resonator is conical except in the region near the edge, where the lower flat surface of the edge is smoothly connected with the circular surface into the resonator. Also, the resonator is tapered by about 0.6%, where the cross section becomes smaller at a closer position to the exit of the resonator. As shown in Fig. 1, the three tone holes are labeled "tone hole 0," "tone hole 1," and "tone hole 2" in turn from the hole closest to the window.

For PIV measurements, a "half model" [namely, as shown in Fig. 1(b), the full model is cut in half along the spanwise direction and the cutting surface is terminated by an acrylic board] was also used. As discussed in Sec. IV A, the intense jet oscillations have been confirmed to occur for this half model like for the full model. Also, Fig. 2 shows the measured sound pressure spectra for half and full models with all opened tone holes at $M = 0.033$, where the measurement point is 500 mm above the window of the recorder and the frequency resolution is 5 Hz. As shown in the figure, the measured fundamental frequency for the half

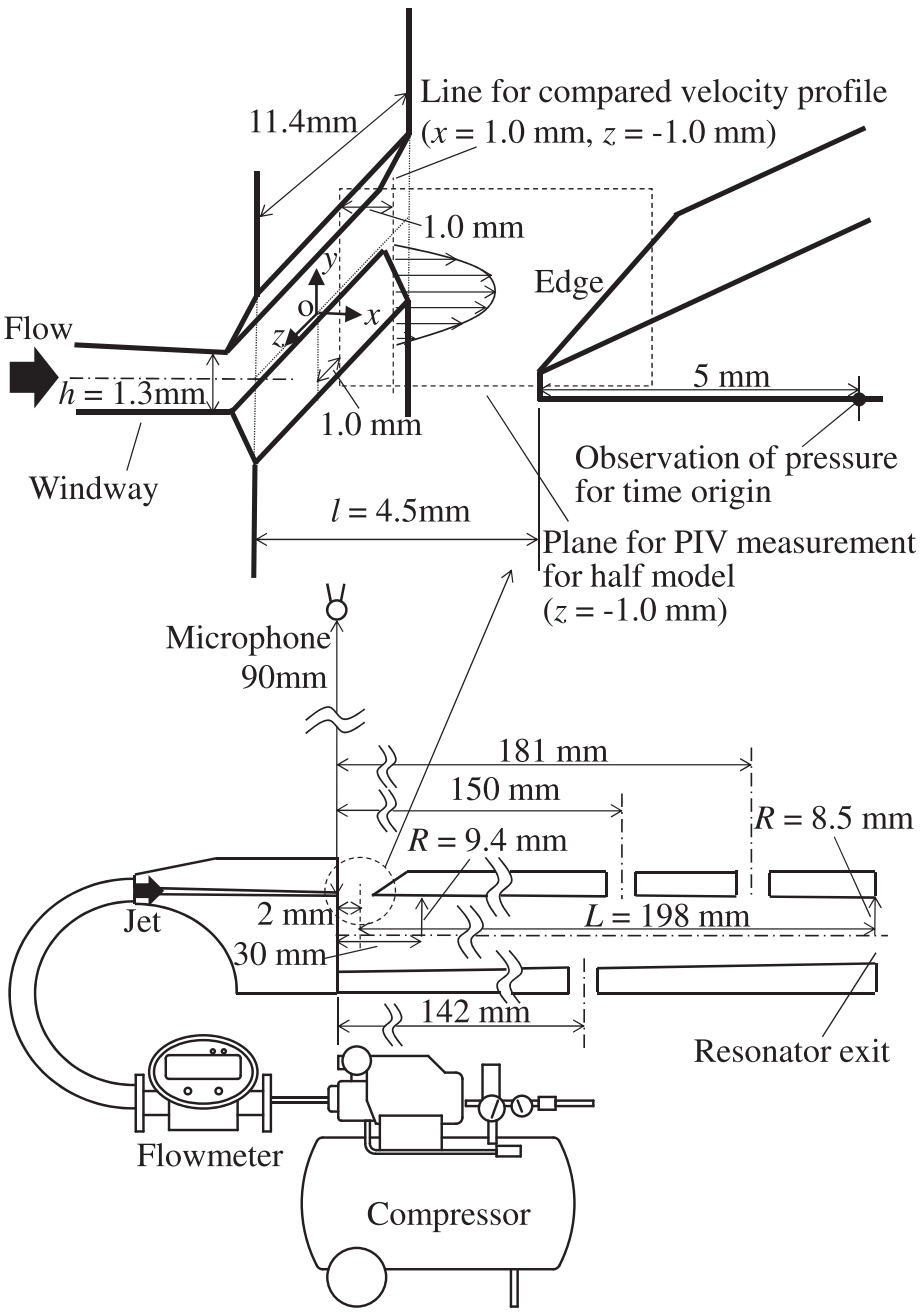

FIG. 3. Configurations of recorder and experimental setup.

TABLE I. Computational and experimental conditions.

Model	Tone holes	Method	Jet velocity U_0 [m/s]	Mach number M	Reynolds number Re
Full model	All open	comp.	8.0, 10.4, 16.7, 32.8	0.024, 0.031, 0.050, 0.099	680, 880, 1420, 2790
		exp.	8.0–39.8	0.024–0.117	680–3390
	Two closed	comp.	10.4	0.031	880
		exp.	8.0–34.1	0.024–0.100	680–2900
	All closed	comp.	10.4	0.031	880
		exp.	8.0–34.1	0.024–0.100	680–2900
Half model	All open	comp.	11.4	0.033	970
		exp.	11.4	0.033	970

model of 800 Hz is in good agreement with that for the full model. Also, the predicted level at the fundamental frequency for the half model approximately agrees with that for the full model, where the level for the half model was corrected by + 6 dB [=20log(2)] on the assumption that the acoustic source becomes smaller by half in proportional to the spanwise edge length and the source is spanwisely coherent. This agreement indicates that the effects of the geometry change on the fluid–acoustic interactions and radiation properties in the far field including this measurement point related with the fundamental tone are negligible. However the spectrum measured for the half model is different at higher harmonic frequencies more than 4000 Hz from that for the model. This is because the acoustic wavelength (86 mm for 4000 Hz) becomes comparable to the length from the recorder to the upper edge of the plate (70 mm) and the effects of the geometry change on the radiation properties and the acoustic shear layer are not negligible for the higher harmonics.

The configuration of the recorder and the experimental setup are shown in Fig. 3. The origin of the coordinate system of the full model is located at the center of the outlet of the windway. For the half model, the origin is set at the boundary between the model and the acrylic board. The streamwise direction in the windway is the x axis, the vertical direction is the y axis, and the spanwise direction intersecting with those two axes is the z axis.

The experimental and computational conditions regarding the state of the tone holes and the cross-sectional average blow-jet velocity are listed in Table I. The jet velocity (U_0) is based on the area at the starting point of the chamfers around the exit of the windway, where the height of the windway (h) is 1.3 mm. To clarify the effects of the state of tone holes on the fluid–acoustic interactions and acoustic fields in the resonator, the computations and experiments were performed for holes in the following three stated: all holes open, two holes closed (tone holes 0 and 1 closed), and all holes closed. Because the recorder is cut shorter in the present paper, the most downstream hole (Tone hole 2) is closer to the exit of resonator and the effects of the statement of this hole are smaller than that in real instruments. However, as discussed in Sec. IV C, we confirmed that the effects of the statement of this hole on the standing wave are not negligible. To discuss the effects of the statement of tone holes more generally, the above-mentioned three cases are discussed in the present paper. The computational model used for opening and closing of tone holes is shown in Fig. 4. To clarify the effects of closing the tone holes, a tone-hole cover with a rectangular shape was put on each tone hole.

The effects of jet velocity (ranging from 8.0 to 32.8 m/s) were computationally investigated by using the full model in the case that all tone holes were open. Moreover, the effects of jet velocity on sound-pressure level in all three cases of tone holes were experimentally measured. This range of jet velocity approximately corresponds to that during an actual performance. Along with the variation of jet velocity, Mach number, $M \equiv U_0/a$, where a is the speed of sound, was changed from 0.024 to 0.099, and the Reynolds number, Re $\equiv U_0 h/\nu$, where ν is kinematic viscosity, was changed from

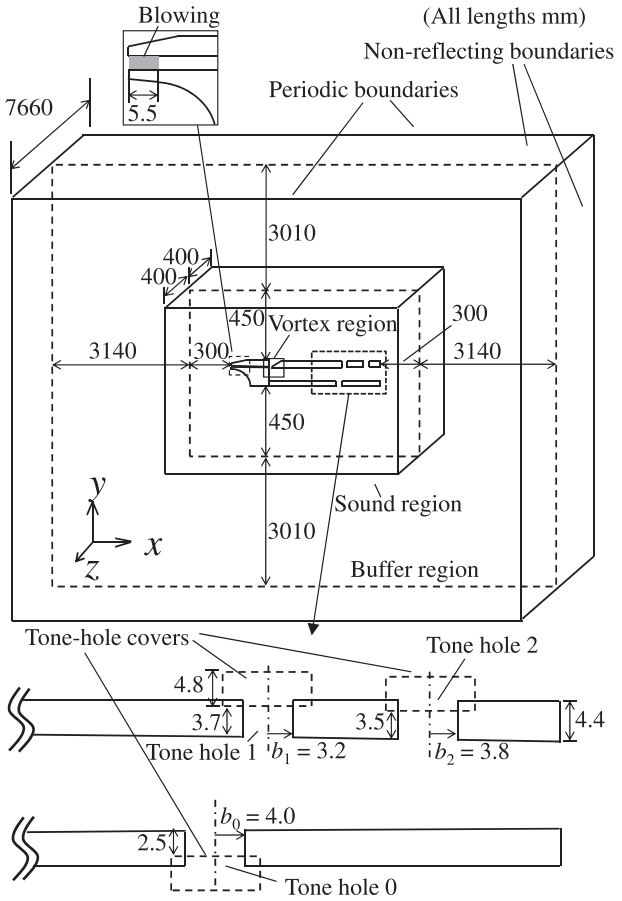

FIG. 4. Computational domain, boundary conditions and models for opening and closing of tone holes.

680 to 2790. The velocity field in the half model was measured at $M = 0.033$ by using by PIV.

B. Experimental methodologies

The experimental setup for measuring jet velocity and sound pressure is shown in Fig. 3. The flow field around the edge in the half model was measured by PIV. In this setup, the flow field was illuminated by a laser (G8000; power: 8 W; KATOKOKEN CO, LTD, Kanagawa, Japan) and observed by high-speed camera (FASTCAM SA1.1; Photron Limited, Tokyo, Japan) at frame rate of 54 kHz, where the whole frame has 256×320 pixels. The flow was seeded with droplets of glycol solvent by a fog generator (FTK-70A; HONDA DYNAMICS Co. Ltd, Osaka, Japan). The sound pressure level was measured in an anechoic room by a non-directional 1/2-in. microphone (RION NA-60; RION CO., LTD., Tokyo, Japan), which was located at distance r from the window of the recorder of 90 mm. This position was set to be out of the recorder to prevent the effects of the flows on the measured sound pressure.

C. Computational methodologies

1. Governing equations and finite-difference formulation

The governing equations used for simulating the interactions between flow and acoustic fields are based on the three-dimensional compressible Navier-Stokes equations. Spatial derivatives are solved by using the sixth-order-accuracy compact finite-difference scheme (fourth-order accuracy at boundaries).[28] Time integration is performed using the third-order-accuracy Runge-Kutta method.

A volume-penalization (VP) method,[29,30] which is a kind of immersed-boundary method,[31] is used to reproduce the flow and acoustic fields around a complex shape of the recorder on a rectangular grid. The penalization term, $\boldsymbol{V}$, is added to right-hand side of the governing equations of the three-dimensional compressible Navier-Stokes equations as follows:

$$\boldsymbol{Q}_t + (\boldsymbol{E} - \boldsymbol{E}_\nu)_x + (\boldsymbol{F} - \boldsymbol{F}_\nu)_y + (\boldsymbol{G} - \boldsymbol{G}_\nu)_z = \boldsymbol{V}, \tag{1}$$

$$\boldsymbol{V} = -(1/\phi - 1)\chi \begin{pmatrix} \partial \rho u_i / \partial x_i \\ 0 \\ 0 \\ 0 \\ 0 \end{pmatrix}, \quad \phi = 0.25, \tag{2}$$

where $\boldsymbol{Q}_t$ is the vector of the conservative variables, $\boldsymbol{E}$, $\boldsymbol{F}$, and $\boldsymbol{G}$ are inviscid flux vectors, $\boldsymbol{E}_\nu$, $\boldsymbol{F}_\nu$, and $\boldsymbol{G}_\nu$ are viscous flux vectors, and ϕ is the porosity of a porous medium, determined so that the sound wave can be reflected almost completely (reflectivity: 99%). The mask function χ is given as

$$\chi = \begin{cases} 1 \ (\text{insiede object}), \\ 0 \ (\text{outside object}). \end{cases} \tag{3}$$

In this simulation, we do not use the specific method to exactly reproduce the curved surface to prevent the growth of the computational, and the surface in the simulation is not exactly smooth. However, this roughness becomes smaller as the grid resolution becomes fine. In these simulations, the predicted flow was confirmed to be smooth along the curved walls of objects using the above-mentioned computational schemes and the grid as discussed in detail in Sec. II C 2. Moreover, by the comparison of the computational and experimental results in Sec. III, the grid resolutions are clarified to be sufficiently fine to reproduce the flow and acoustic field in and around the recorder.

To reduce computational cost, LES were performed for the reproduction of the flow fields in the recorder. In the simulations, no explicit subgrid-scale (SGS) model was used. The turbulent energy in the grid-scale (GS) that should be transferred to SGS eddies is dissipated by a 10th-order spatial filter as described below. A number of studies[32–37] have shown that the above-mentioned computational method, which combines low-dissipation discretization schemes and explicit filtering, correctly reproduces turbulent flows. This filter, which is given as

$$\alpha_f \hat{\psi}_{i-1} + \hat{\psi}_i + \alpha_f \hat{\psi}_{i+1} = \sum_{n=0}^{5} \frac{a_n}{2} (\psi_{i+n} + \psi_{i-n}), \tag{4}$$

where ψ is a conservative quantity and $\hat{\psi}$ is the filtered quantity, also removes numerical instabilities.[34] Coefficient a_n has the same value as that used by Gaitonde and Visbal,[38] and the value of α_f is 0.45.

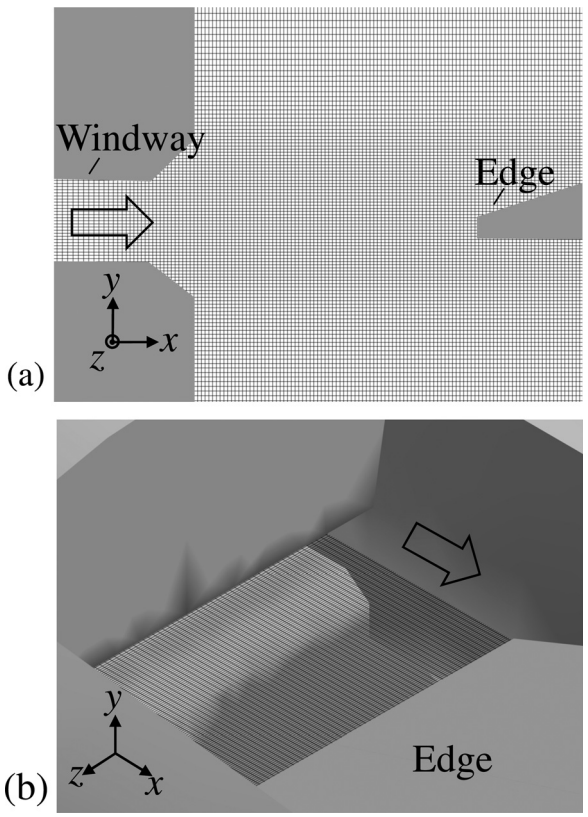

FIG. 5. Computational grid near windway exit and edge: (a) grid on x-y cross section ($z = 0$) and (b) grid on x-z cross section ($y = 0$).

2. Computational grid

The computational domain (shown in Fig. 4) is divided into three regions: a vortex region, a sound region, and a buffer region having different grid spacings, while the grid spacing is smoothly changed to prevent spurious acoustic reflections near the boundary of different regions. The computational grid is rectangular (as mentioned above). The computational grid in the x-y cross section ($z = 0$) and that in the x-z cross section ($y = 0$) near the window exit and edge are shown in Figs. 5(a) and 5(b), respectively. The total number of grid points is approximately 8.2×10^7.

In the vortex region, the grid spacing around the window exit and edge is set to $\Delta x/h = \Delta y/h = 0.04$ and $\Delta z_{\min}/h = 0.11$. These spacings are sufficiently fine to capture oscillations of the jet and vortices around the edge, where the jet minimum width is approximately h, and the scale of dominant two-dimensional vortical structures is $0.5h$. The spanwise resolution is relatively rough in comparison with those in other directions. However, preliminarily, it has been confirmed that the flow in the channel is laminar and the spanwise variation is negligible. Also, as discussed later in Sec. IV B 2, the intensification of the sound pressure fluctuations at high frequencies related with the turbulent flow is correctly predicted with comparison with the measured result. Therefore, the spanwise resolution is also sufficient to predict the flow and acoustic fields in and around the recorder. It is thus concluded that the present computational grid in the vortex region is sufficiently fine to capture the vortical structures related with sound. Because the fundamental acoustic wavelength is much larger ($330h$), the acoustic waves in the vortex region can also be captured.

In the sound region, although the grid spacing ($\Delta/h \leq 32$) is rougher than that in the vortex region, it is sufficiently fine to capture the propagation of acoustic waves. In this computation, more than 10 grid points are used per fundamental wavelength of first regime ($\lambda_p = 330h$). Particularly, in the resonator, the resolution Δ is finer than $0.7h$, where 470 grid points are used per fundamental wavelength of the first mode λ_p. At the point of $x = 0$, $y = 69h$ (90 mm), and $z = 0$ where the acoustic pressure fluctuations were sampled, the resolution Δ is finer than $4h$ (80 grid points per λ_p). Therefore, the acoustic propagation at higher harmonic frequencies up to 10 f_p can be predicted using the above-mentioned high-order numerical schemes. Also, in the buffer region, to weaken acoustic waves near the artificial outflow boundaries, the grid is stretched.

3. Boundary condition

The boundary conditions of the computation are shown in Fig. 4. Non-reflecting boundaries[39–41] are used at boundaries of the x and y directions, and periodic boundary conditions are adopted in the z direction. To reproduce the jet in the windway, the velocity is set to be a given blowing velocity in the inlet region of the windway, as shown in gray color in Fig. 4, where the blowing velocity was determined to set the jet velocity at the exit of the windway as shown in Table I. For the objects such as a recorder, tone-hole covers, and an

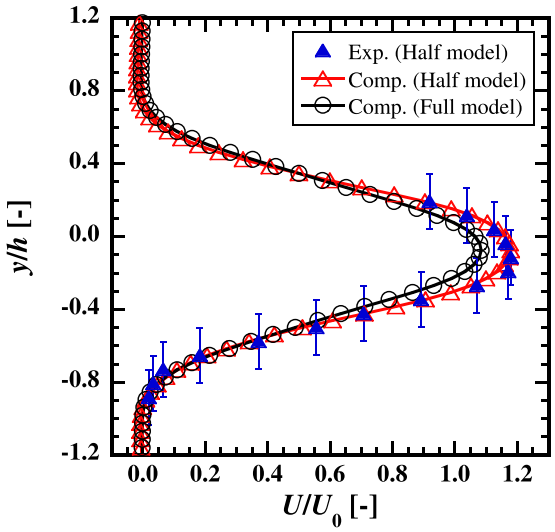

FIG. 6. (Color online) Predicted and measured velocity profiles at $M = 0.033$ in case of all holes open ($x/h = 0.77$, $z/h = -0.77$).

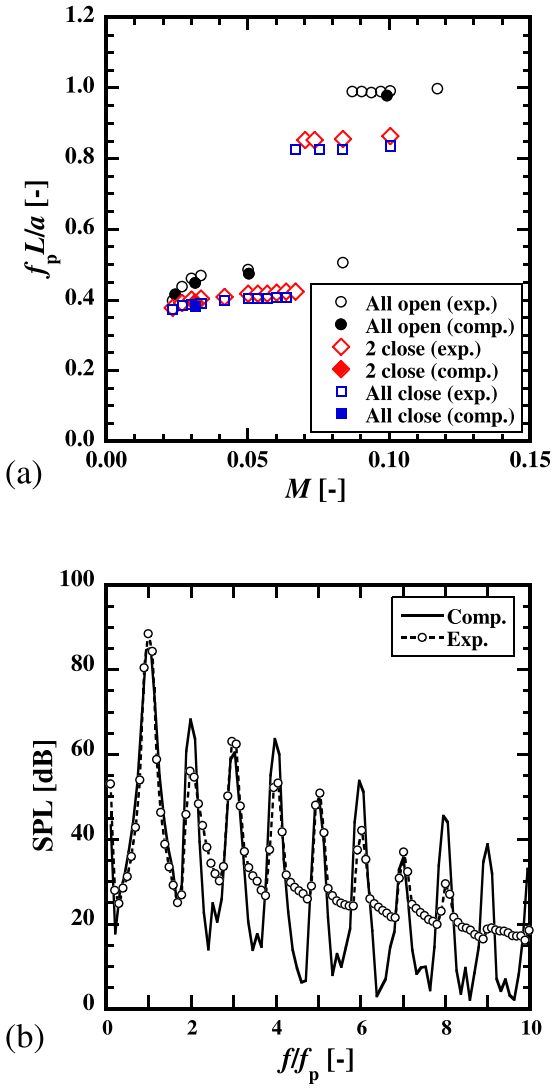

FIG. 7. (Color online) (a) Variation of frequency of dominant tone with Mach number. (b) Predicted and measured sound spectra in case of all holes open at $M = 0.031$ at $x = 0$, $y = 69h$ (90 mm), and $z = 0$.

TABLE II. Predicted peak frequencies and non–dimensional velocity.

Tone holes	Mach number M	Peak frequencies f_p [Hz]	Non–dimensional velocity V
All open	0.024, 0.031, 0.050, 0.099	694, 747, 791, 1631	2.58, 2.39, 2.26, 1.10
Two closed	0.031	654	2.73
All closed	0.031	635	2.82

acrylic plate, the above-mentioned mask function is set to $\chi = 1$, and the velocity is set to zero.

III. VALIDATION OF COMPUTATIONAL METHODS

A. Flow fields

To validate the computational accuracy regarding flow fields, the predicted flow field in the downstream of the windway exit is compared with that measured for the half model. Figure 6 shows the measured and predicted mean velocity profiles at $x/h = 0.77$ and $z/h = -0.77$ in the downstream of the windway exit for the half model along with the predicted that for the full model at $M = 0.033$ with all opened tone holes. The error bars on the measurements are also indicated in the figure. The errors were mainly due to the difficulty of identifying the origin of the coordinate system.

The predicted and measured profiles for the half model are slightly different around the maximum speed by about 8% in comparison with that predicted for the full model as shown in Fig. 6. This difference occurs possibly because the spread of the momentum is slightly suppressed by the weakening of the jet oscillations due to the acrylic board in the half model. However, as discussed in Sec. II A, the effects of the geometry change between the full and half models on the self-sustained oscillations related with the fundamental tone are not significant as a whole.

As shown in Fig. 6, the predicted profile for the half model is in good agreement with that measured for the same model (half model). This agreement means that this simulation have the ability to predict the flow field accurately.

B. Sound fields

The effects of Mach number on the non-dimensionalized frequency of dominant tone (fundamental frequency), f_pL/a, where L is the distance from the window to the resonator exit (see Fig. 3), are shown in Fig. 7(a). It has been confirmed in the experiments that the effects of the hysteresis on the threshold of the jet velocity between the first and second modes are negligible in this model, where the threshold differs by less than 1 m/s in the case of acceleration and in that of deceleration. The measured data in Fig. 7(a) were obtained

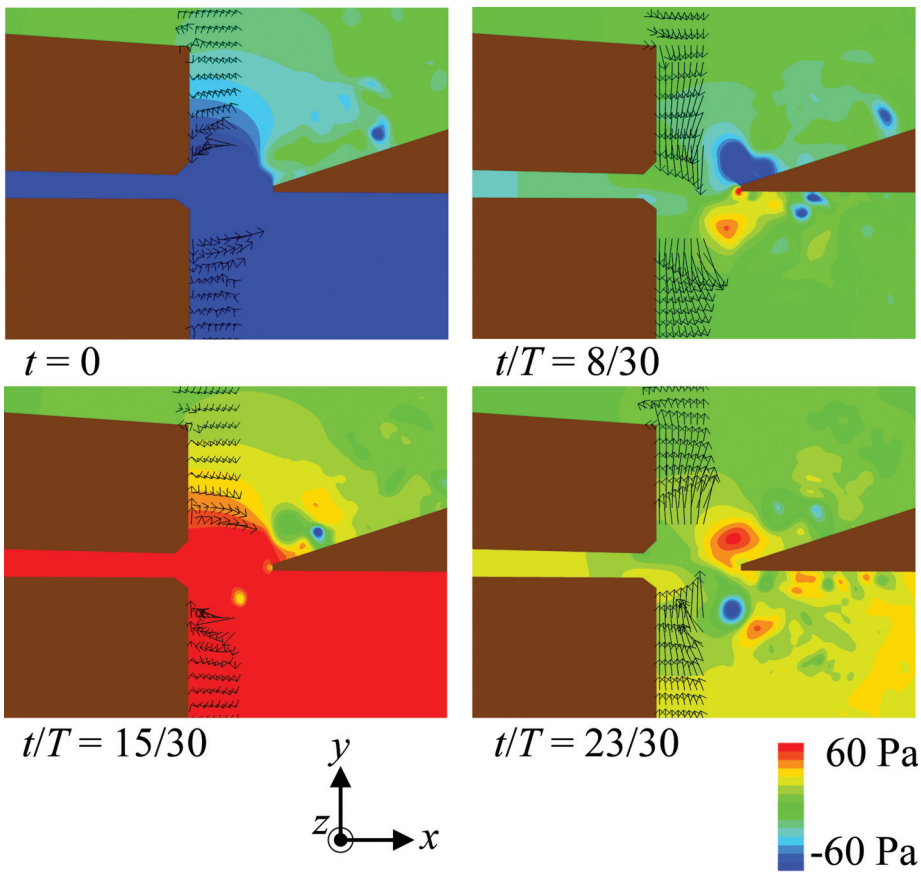

FIG. 8. Contours of pressure-fluctuation and velocity-fluctuation vectors ($z = 0$) at $M = 0.031$ in case of all holes open, where T is time period.

as the velocity was accelerated. In the computation, the velocity is set to zero in the initial field and the jet velocity is accelerated in the duration of computational development like in the experiments. It is interesting to predict the hysteretic behavior of the instrument in the computation. However, it is difficult in this model due to the small hysteretic range of the velocity.

As Mach number increases, the frequency becomes higher and jumps from the first mode to the second mode at $M = 0.087$, where the first and second modes correspond to the acoustic half-wavelength and one-wavelength modes of the resonator, respectively. Also, the frequency becomes lower as more tone holes are closed. These tendencies are correctly captured in the present simulations. The effects of the state of the holes on the acoustic fields in the resonator are discussed in Sec. IV C.

Predicted and measured sound-pressure spectra at $x = 0$, $y = 69h$ (90 mm), and $z = 0$ at $M = 0.031$ in the case of all tone holes open (where frequency resolution is approximately $f_p/10$) are shown in Fig. 7(b). The measurement point is out of the recorder as shown in Fig. 3. Also, this somewhat rough frequency resolution is related to the computational cost, where it takes 100 nodes (1 node/16 processors) and 230 h for the present case, because the time step is very fine ($\Delta t = 5.8 \times 10^{-8}$ s) in the present direct simulations of flow and acoustic fields. The better frequency resolution is a future subject. The predicted level of a dominant tone at frequency f_p agrees well with the measured one, and the generation of higher harmonics is correctly predicted by the proposed computation. As stated in the discussions of flow fields in Sec. III A, the present computations adequately predict the flow and acoustic fields in the recorder models.

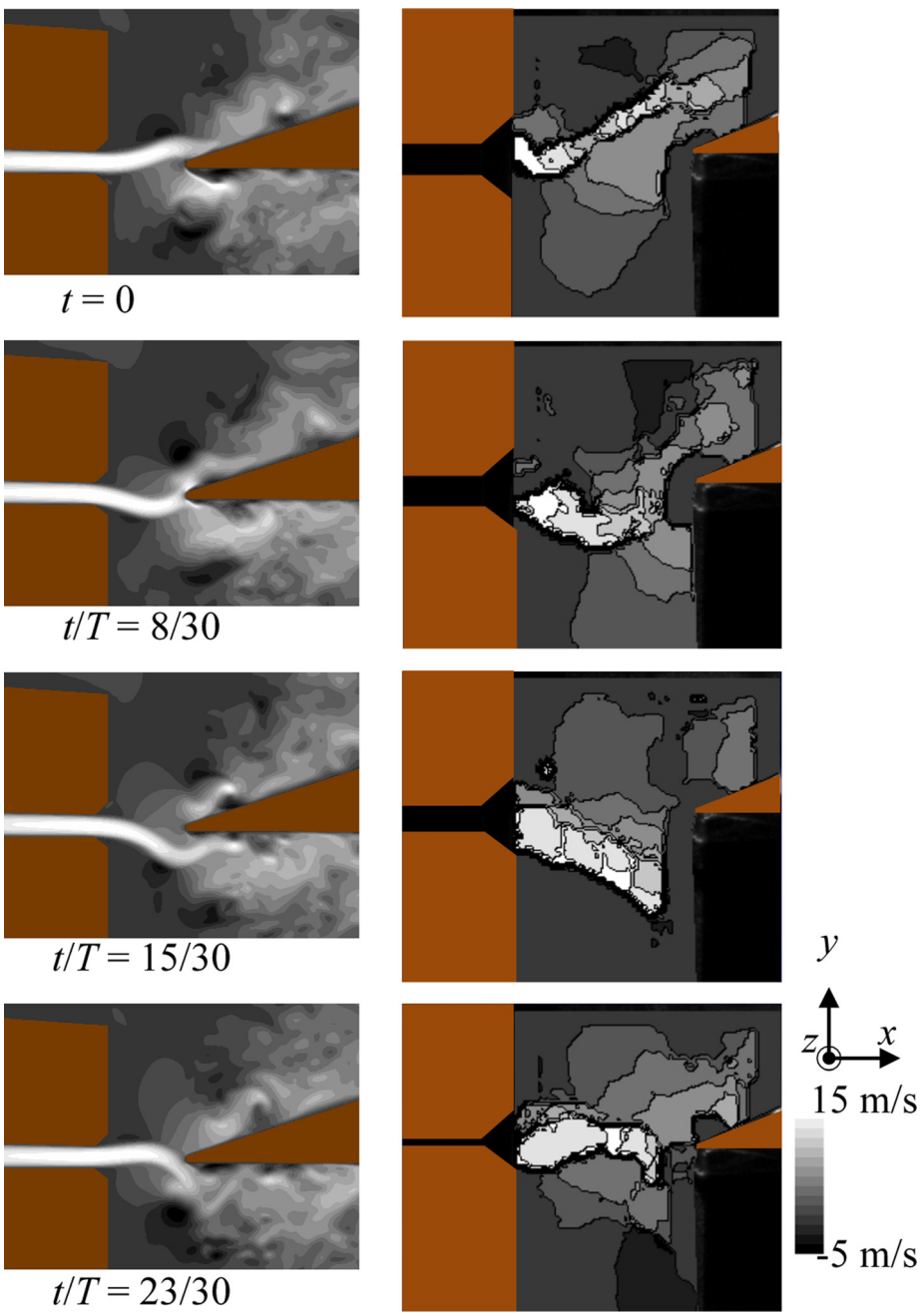

FIG. 9. (Color online) Contours of streamwise velocity in case of all holes open, where T is time period. Predicted field for full model at $M = 0.031$ along $z = 0.0$ (left) and measured field for half model at $M = 0.033$ along $z = -0.77$ (right).

IV. RESULTS AND DISCUSSION

A. Mechanism of self-sustained oscillations

Table II shows the predicted peak frequencies and dimensionless velocity $V \equiv U_0/fl$ based on the window length and the jet velocity. The mechanism of self-sustained oscillations in an actual recorder is revealed by using predicted flow and acoustic fields at $M = 0.031$ in the all-tone-holes-open case. Contours of pressure with a time-averaged component subtracted, p' (pressure-fluctuation) and velocity-fluctuation vectors around the exit of the windway and edge are shown in Fig. 8. In the figure, the vectors are shown in the region where the effects of the fluid-dynamical structures (such as vortices) on the fields are small, and the intensity and direction of acoustic particle velocity are indicated. The time origin ($t = 0$) is the time that the pressure becomes lowest at a point 5 mm from the vertex of the edge (on the bottom of the edge) in fundamental time period T (the point is shown in the top figure in Fig. 3).

At $t/T = 8/30$ in Fig. 8, the highest downward particle velocity is induced. Predicted contours of instantaneous streamwise velocity ($M = 0.031$, $z = 0$) are shown in Fig. 9 along with those measured ($M = 0.033$, $z/h = -0.077$). Both predicted and measured figures show the intense jet oscillations. At $t/T = 8/30$, the jet starts to be deflected downward because the acoustic particle velocity is highest. This mechanism is consistent with experimental results reported by Coltman.[4,19] Moreover, these small deflections (disturbances) are developed and convected downstream, and as shown in Fig. 9, the downward deflection of the jet becomes most intense at $t/T = 15/30$. As a result, air flows into the resonator on mass and compresses the air in it. In the opposite phase, namely, at $t = 0$, the air in the resonator expands when the upward deflection of the jet is largest. This phase of pressure fluctuations with respect to the jet-crossing time is consistent with the above-mentioned jet-drive model.[4] These pressure fluctuations induce a dipolar acoustic field around the edge. On the other hand, additional time for the pressure to rise (by the loss of the momentum fluctuations induced after the deflection of the jet) is needed under the assumption of the momentum-transfer model,[3] although the compression occurs at the same time as the deflection of the jet.

Contours of vorticity are shown in Fig. 10(a). As shown in the figure, the oscillations of the jet generate vortices around the edge. Vortical structures at $t/T = 8/30$ elucidated by the iso-surfaces of the second invariant of velocity-gradient tensor $Q = \|\Omega\|^2 - \|S\|^2$, where Ω and S are anti-symmetric and symmetric parts, are shown in Fig. 10(b). Regions with $Q > 0$ represent vortex tubes. As shown in Figs. 10(a) and 10(b), two-dimensional vortical structures are shed above the edge at $t/T = 8/30$. Although the deformation of these two-dimensional vortices by collision with the edge could radiate an expansion wave by the analogy based on the mechanism of acoustic radiation in cavity tone,[36] such an intense expansion wave is not apparent above the edge. This result also supports the conclusion that the radiation due to the jet oscillations based on the jet-drive model[4] is the most suitable for the sound-producing mechanism of

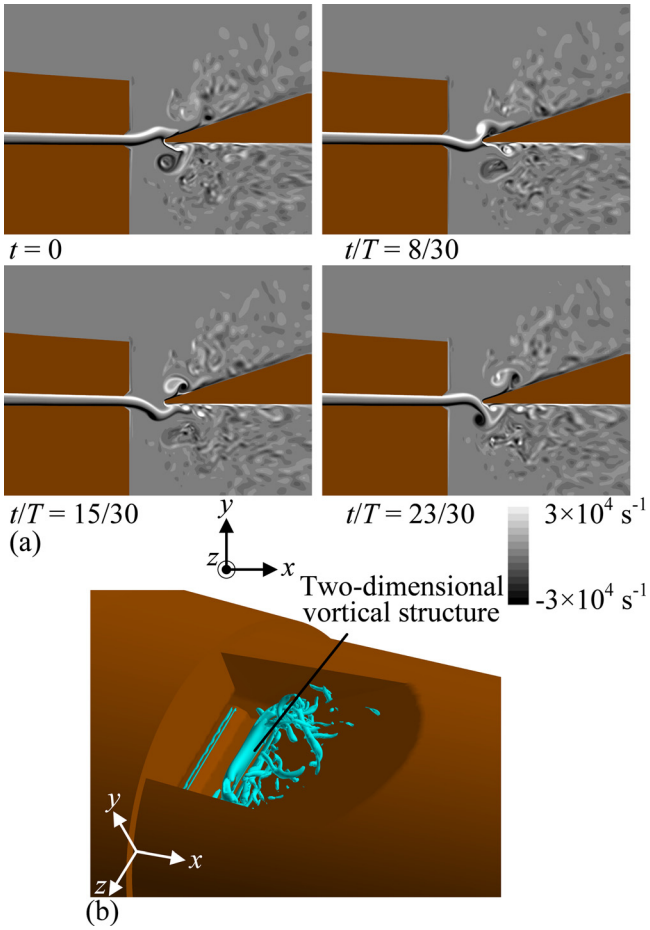

FIG. 10. (Color online) Vortical structures at $M = 0.031$ in case of all holes open, where T is time period. (a) Contours of vorticity ($z = 0$). (b) Iso-surfaces of second invariant $Q/(U_0/h)^2 = 1.5$ at $t/T = 8/30$.

the fundamental tone of a recorder. However, as discussed in Sec. IV B, the vortices near the edge affect the higher harmonics.

In this section, the following feedback-loop mechanism was clarified to sustain the acoustic resonance for the fundamental tone. The disturbances are generated due to the acoustic particle velocity due to the acoustic resonance, the disturbances are developed into the intense deflection of the jet, and this deflection leads to the compression and expansion of air in the resonator. These fluctuations sustain the acoustic resonance, and generate the acoustic particle velocity again.

B. Effects of state of holes and jet velocity on fluid–acoustic interactions

1. Effects of state of tone holes

Contours of pressure-fluctuation and velocity-fluctuation vectors in the case of all holes closed at $M = 0.031$ and contours of streamwise velocity when downward particle velocity becomes highest ($t/T = 8/30$) are shown in Figs. 11(a) and 11(b), respectively. Likewise, those when the most intense downward deflection of the jet occurs are shown in Figs. 11(c) and 11(d), respectively. These figures clarify that the jet starts to be deflected at the former time and that air in the

resonator is compressed at the latter time. This feedback-loop mechanism has been also confirmed by the predicted results for the case that two holes are closed. It is therefore confirmed that the mechanism of the feedback loop proposed in Sec. IV A is independent of the state of tone holes.

2. Effects of jet velocity

Contours of pressure-fluctuation and velocity-fluctuation vectors in the case of all tone holes open at $M = 0.050$ are shown in Fig. 12 in the same way as those in Sec. IV B 1. As shown in the figure, the above-mentioned feedback-loop mechanism is also confirmed to be independent of Mach number. However, the time of the most-intense downward deflection of the jet becomes shorter from $t/T = 16/30$ to 13/30 as Mach number increases from $M = 0.024$ to 0.050 (Re = 680–1420), while the highest downward particle velocity is generated and acoustic feedback occurs at approximately the same time as $t/T = 8/30$. This variation of time difference between the acoustic feedback and the most downward deflection of the jet is because the disturbances are more swiftly convected and intensified downstream as Mach number increases, while the fluctuation of particle velocity is determined acoustically by standing waves in the resonator. Moreover, this variation of the time difference between the acoustic feedback and the generation of the acoustic power is related with the fundamental frequency (as discussed in Sec. IV C 3).

Vortical structures at $M = 0.099$ and $t/T = 8/30$, where T is the time period corresponding to the half-wavelength (first) mode of the resonator, are shown in Fig. 13. At this Mach number, the Reynolds number based on the windway height and the jet velocity is 2790 and that based on the windway length is 9660. Although the second mode corresponding to the one-wavelength acoustic mode of the resonator becomes dominant in the sound-pressure spectra at $M = 0.099$, the oscillations of the jet corresponding to the half-wavelength mode are still intense. Therefore, the jet oscillations are repetitive during the period corresponding to this mode. Iso-surfaces of the second invariant are shown in Fig. 13(a), and contours of vorticity ($z = 0$) are shown in Fig. 13(b).

As shown in Fig. 13, the fine-scale two-dimensional vortices become apparent in comparison with the flow at $M = 0.031$ (as shown in Fig. 10). These two-dimensional vortices support the fact that the flow is laminar in the channel as mentioned in Sec. II C 2. Also, small-scale streamwise vortices are also formed in the spanwisely entire region along the edge as shown in Fig. 13(a), while those are formed sparsely at $M = 0.031$ as shown in Fig. 10(b). This indicates that a turbulent transition of the flow is more

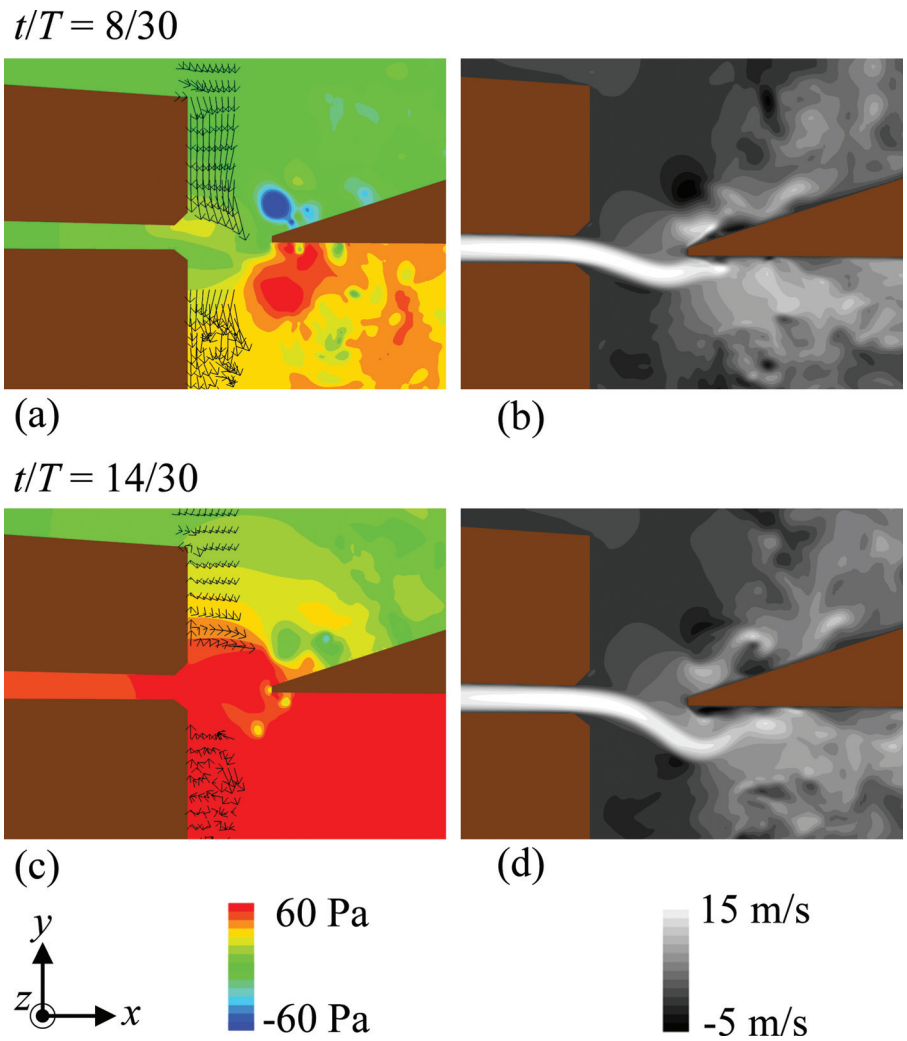

FIG. 11. Acoustic feedback and compression of an air in resonator ($z = 0$) at $M = 0.031$ in case of all holes closed at $t/T = 8/30$ and 14/30, where acoustic feedback due to the highest downward particle velocity occurs at $t/T = 8/30$, and compression of air due to the most-intense deflection occurs at $t/T = 14/30$. (a) Contours of pressure-fluctuation and velocity-fluctuation vectors at $t/T = 8/30$. (b) Contours of streamwise velocity at $t/T = 8/30$. (c) Contours of pressure-fluctuation and velocity-fluctuation vectors at $t/T = 14/30$. (d) Contours of streamwise velocity at $t/T = 14/30$.

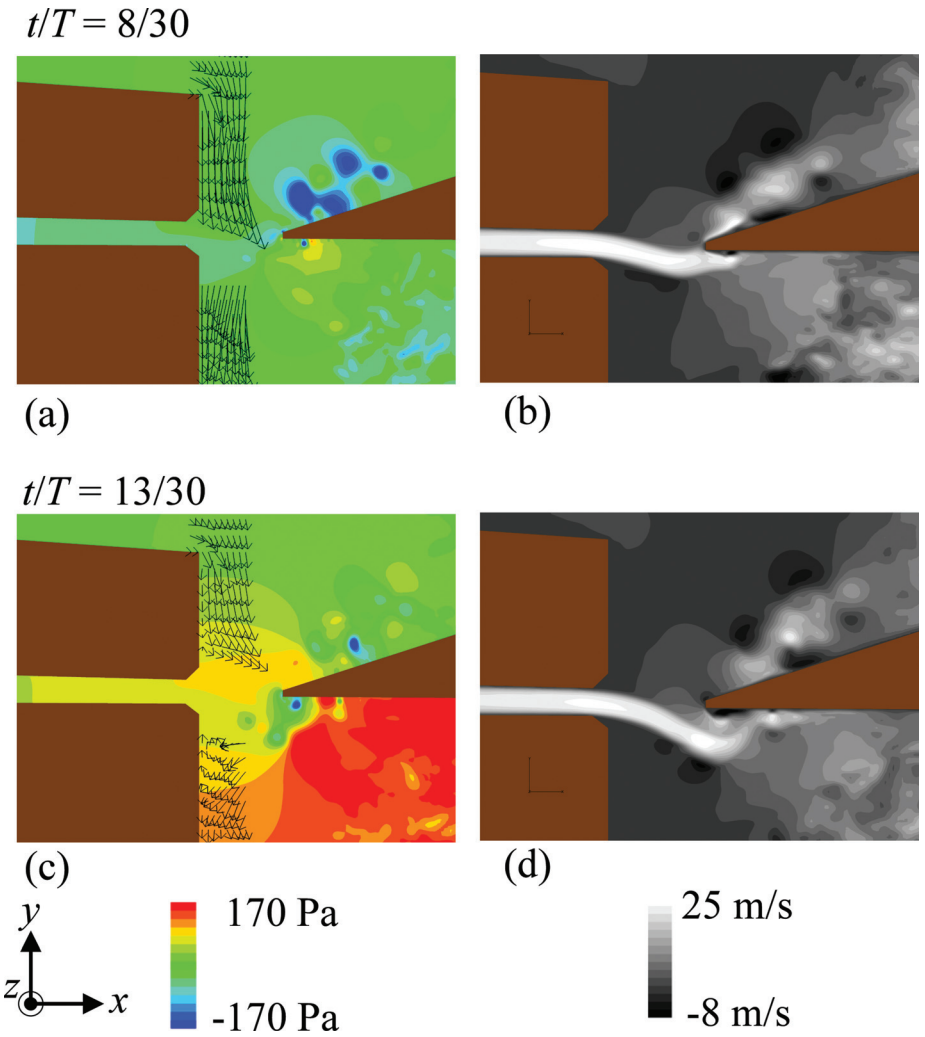

FIG. 12. Acoustic feedback and compression of an air in resonator at $M = 0.050$ in case of all holes open at $t/T = 8/30$ and 13/30 ($z = 0$), where the acoustic feedback due to the highest downward particle velocity occurs at $t/T = 8/30$ and compression of air due to the most-intense deflection occurs at $t/T = 13/30$. (a) Contours of pressure-fluctuation and velocity-fluctuation vectors at $t/T = 8/30$. (b) Contours of streamwise velocity at $t/T = 8/30$. (c) Contours of pressure-fluctuation and velocity-fluctuation vectors at $t/T = 13/30$. (d) Contours of streamwise velocity at $t/T = 13/30$.

developed near the edge as the two-dimensional vortices pass the edge than at $M = 0.031$.

Figure 14(a) shows the power spectra of velocity fluctuations at $M = 0.031$ and 0.099 at $x/h = 3.1$ (4.0 mm), $y/h = 3.5$ (4.6 mm), $z = 0$, where this height (y) is corresponding to that for the highest amplitude of velocity fluctuations. As shown in Fig. 14(a), the levels at higher harmonic frequencies around $f/f_p = 4$–8 become much larger for the higher Mach number of $M = 0.099$ in comparison with those for $M = 0.031$. This intensification at high harmonic frequencies is corresponding to the occurrence of the above-mentioned fine two-dimensional vortices as shown in Fig. 13.

Predicted and measured sound-pressure spectra at $M = 0.031$ and 0.099 in the case of all tone holes open are shown in Fig. 14(b). As shown in the figure, the overall background level becomes larger at a high frequency around $f/f_p > 2$ when Mach number increases from 0.031 to 0.099. This intensification is correctly predicted along with the measured sound pressure level and due to the increase of the jet velocity and the above-mentioned developed turbulent flow. Moreover, the levels at higher harmonic frequencies around $f/f_p = 4$–8 become higher at $M = 0.099$ along with the above-mentioned power spectrum of velocity fluctuations. This result means that this intensification of the sound pressure at higher harmonic frequencies is due to the above-mentioned fine two-dimensional vortices. The relationship between the change of the mode and these fine two-dimensional vortices is a future subject.

As discussed in this subsection, the vortices near the edge affect the acoustic radiation particularly at the levels of the higher harmonics or background sound at high Mach number. These effects are consistent with those reported in a past study.[14]

C. Acoustic fields in resonator

1. Standing waves in resonator

Contours of pressure-fluctuation at $t = 0$ for the three tone-hole cases, i.e., (a) all holes open, (b) two holes closed, and (c) all holes closed, are shown in Fig. 15. In cases (a) and (b), the standing wave maintains intensity between the window and the open hole closest to the window; in contrast, in case (c), it maintains intensity between the window and the resonator exit. By adaptation of transmission line theory for the wind instrument ending in a section provided with several open side holes, Benade[42,43] clarified that the highest open hole acts as the termination of the upper closed-hole part. In this study, the effects of the statement of tone holes on the impedance and open end corrections were

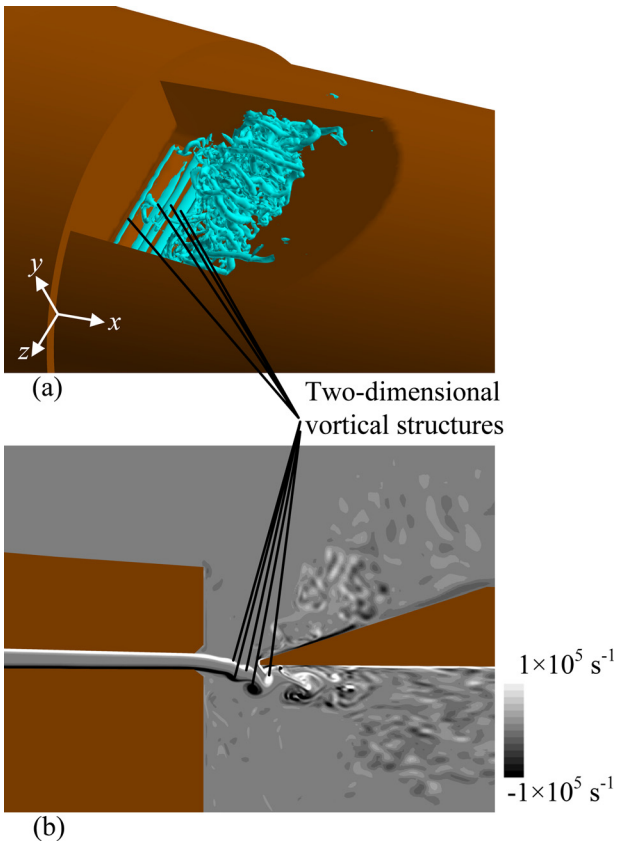

FIG. 13. (Color online) Vortical structures at $t/T = 8/30$ at $M = 0.099$ in case of all holes open, where T is a time period corresponding to a half-wavelength mode. (a) Iso-surfaces of second invariant $Q/(U_0/h)^2 = 0.6$. (b) Contours of vorticity ($z = 0$).

theoretically investigated. The present computational results support this result.

The positions of the pressure anti-node and node of the standing wave were identified as shown in Fig. 15. In identifying the position of the pressure anti-node, it is assumed that the sound pressure level is most intense at that point. The position of the pressure node near the tone holes or resonator exit was estimated by the acoustic wavelength based on the fundamental frequency and the above-mentioned position of the pressure anti-node.

Figure 16 shows the velocity vectors and contours of the spanwise (z-dir) vorticity along $z = 0$ at $t/T = 0$ and 0.5 at $M = 0.031$ for the above-mentioned three tone-hole cases. In the region away from the holes in the resonator, the steady streamwise velocity is dominant in comparison with the acoustic particle velocity, where the steady streamwise velocity is about 0.8 m/s (8% of the jet velocity U_0). In the regions near the holes, the upward and downward velocity fluctuations due to acoustic particle velocity occur along with the pressure fluctuations of the standing wave in the resonator. These fluctuations induce the intense vorticity along the wall near the hole. Particularly, the intense velocity fluctuations and vorticity are apparent near the tone hole 0 with all opened holes [(a) in Fig. 16] and tone hole 2 with two closed holes [(b) in Fig. 16].

These results support the above-mentioned region of the standing wave between the window and the open tone hole closest to the window.

2. Effects of jet velocity and state of tone holes on anti-nodes and nodes

In this subsection, the effects of jet velocity and state of tone holes on standing waves related with the first mode. Figure 17 shows the effects of the jet velocity and the state of tone holes on the predicted position of the pressure node near the tone holes or the resonator exit. In this figure, the position of the pressure node predicted by the transmission line theory as mentioned in the previous subsection is also shown [using Eq. (38) in the literature by Benade[43]]. Although the position predicted by the transmission line theory is slightly smaller, the qualitative effects of the statement of the tone holes and the Mach number are consistent in both predictions. As shown in this figure, the effects of the Mach number on the position of the pressure node are

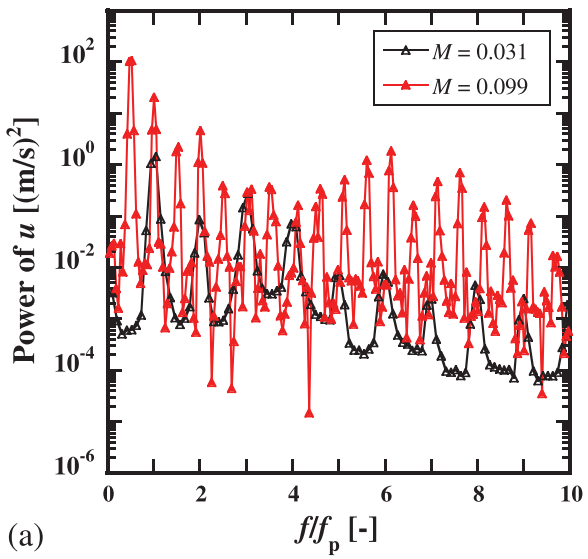

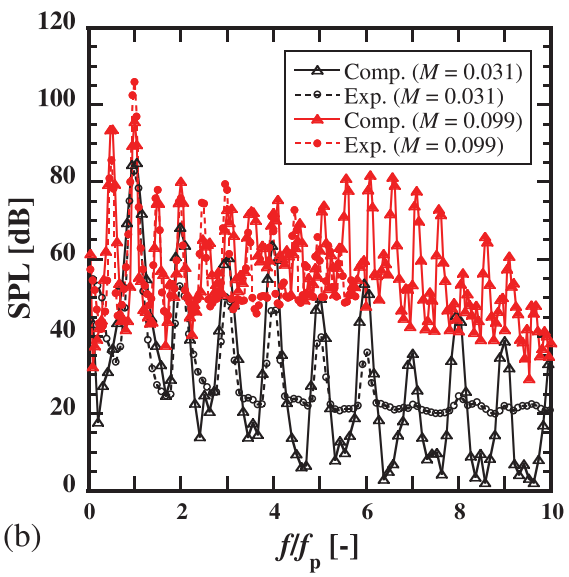

FIG. 14. Spectra in case of all holes open at $M = 0.031$ and 0.099. (a) Predicted power spectra of streamwise velocity fluctuations at $x/h = 3.1$ (4.0 mm), $y/h = 3.5$ (4.6 mm), $z = 0$. (b) Predicted and measured sound spectra at $x = 0$, $y = 69h$ (90 mm), and $z = 0$.

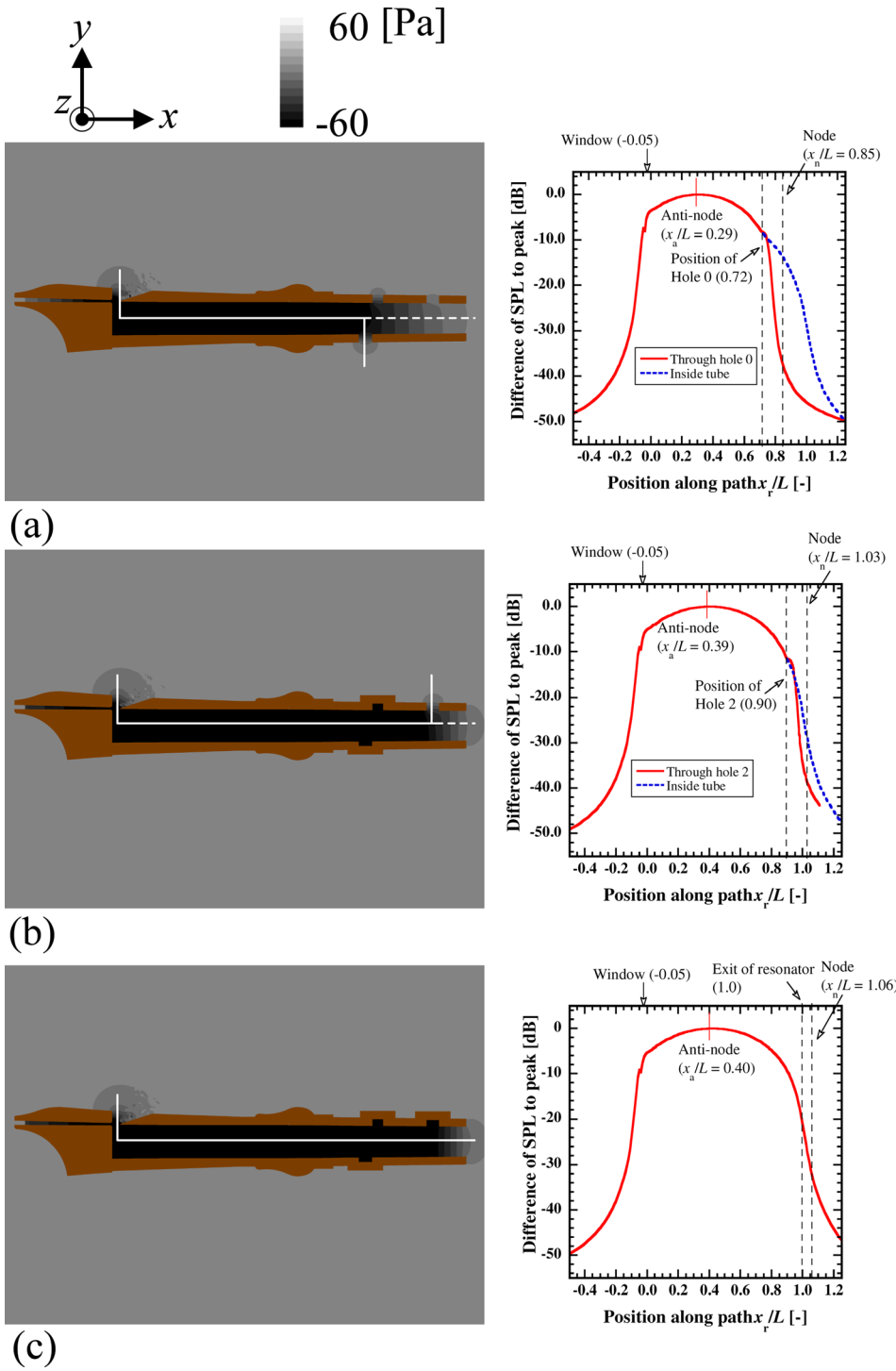

FIG. 15. (Color online) Contours of pressure-fluctuation along $z = 0$ at $M = 0.031$ ($t = 0$) (left). Distributions of sound pressure level along paths indicated in left figure (right). (a) All holes open, (b) two holes closed, and (c) all holes closed.

negligible in both predictions. Also, as more tone holes become closed, the node is displaced from the window.

Variation of positions of the pressure node, x_n, and anti-node, x_a, in accordance with the state of tone holes at $M = 0.031$ is shown in Fig. 18(a). As more tone holes become closed, the node and anti-node are both displaced from the window because the proposed path of the standing waves becomes longer, where another node exists near the window.

Variation of x_n and x_a in accordance with Mach number in the case of all holes open is shown in Fig. 18(b). It is clear that only the anti-node becomes displaced from the window at higher Mach number, while the position of the node is approximately constant. This result means that the time delay of acoustic reflection at the window (as discussed in detail below) becomes shorter at higher Mach number, while the effects of Mach number on the acoustic behaviors near the tone holes and the exits of the resonator are negligible (as mentioned above). Also, as Mach number increases, the distance from the anti-node to the node at tone hole 0 decreases. This finding is consistent with the fact that the fundamental frequency becomes higher as Mach number increases [as shown in Fig. 7(a)].

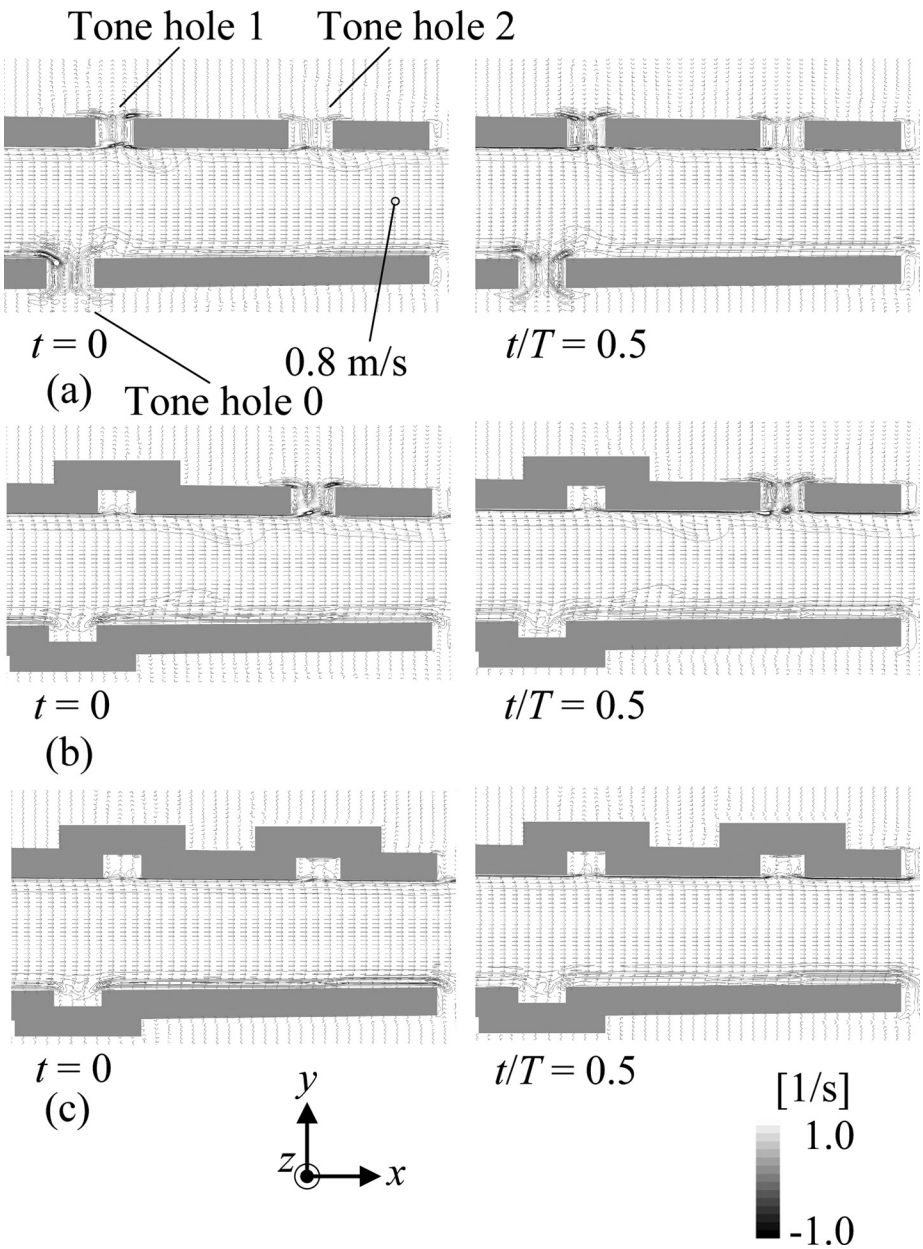

FIG. 16. Velocity vectors and contours of spanwise vorticity along $z = 0$ at $M = 0.031$ (Left: $t = 0$, Right: $t/T = 0.5$). (a) All holes open, (b) two holes closed, and (c) all holes closed.

3. Effects of jet velocity on time delay at window

The above-mentioned time delay of the acoustic reflection around the window, T_w, is given as

$$T_w/T = 0.5 - 2L_u/(aT), \tag{5}$$

where L_u is the distance from the window to the anti-node, and T is the time period corresponding to the first (half-wavelength) mode. This time delay is related with the impedance of the mouth of an instrument or a side branch used by Coltman,[44] Kooijman *et al.*,[45] Graf and Ziada,[46] and Tonon *et al.*[47] Variation of this time delay with Mach number is shown with circular markers in Fig. 19, which indicates that the time delay becomes shorter as Mach number increases. This time difference is related with the determination of the fundamental frequency, where the fundamental frequency becomes higher at a higher Mach number.

This time delay is dependent on the time difference between the acoustic feedback and the generation of the acoustic power (as discussed in Sec. IV A). The time difference between the time of generation of downward disturbances (due to increasing acoustic particle velocity) and the time of the most-intense downward deflection of the jet was computed from the predicted flow fields and is also shown with triangular markers in Fig. 19.

Like the above-mentioned time delay of acoustic reflection, this time difference decreases as the Mach number of jet velocity increases because the disturbances due to acoustic feedback are more swiftly convected and intensified downstream. However, as shown in Fig. 19, the variation of the time difference of the acoustic reflection (circular markers) from $M = 0.031$ to 0.099 is smaller than that of the convective time difference (triangular markers), where the convective time difference is approximately in inverse proportion with the jet velocity. The difference of the variation between these two times is possibly related with a minor increase of the fundamental frequency around the passive resonance frequency of the resonator.[6] This should be discussed in detail in the future.

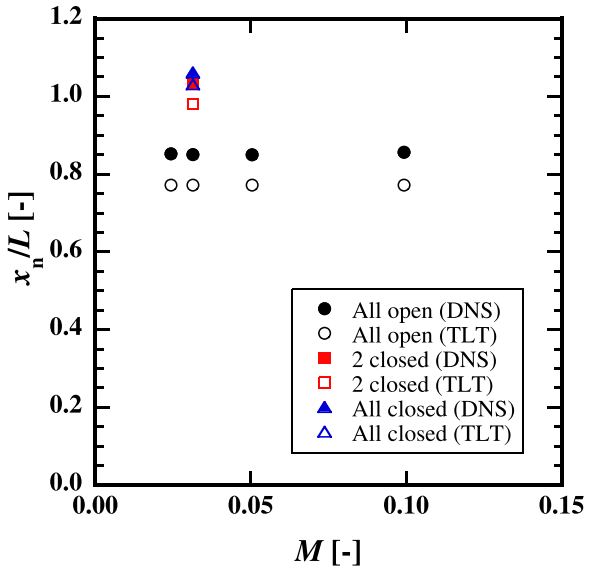

FIG. 17. (Color online) The positions of pressure node near the tone hole or resonator exit predicted by the present direct numerical simulation and those predicted by transmission line theory (TLT) (Ref. 43).

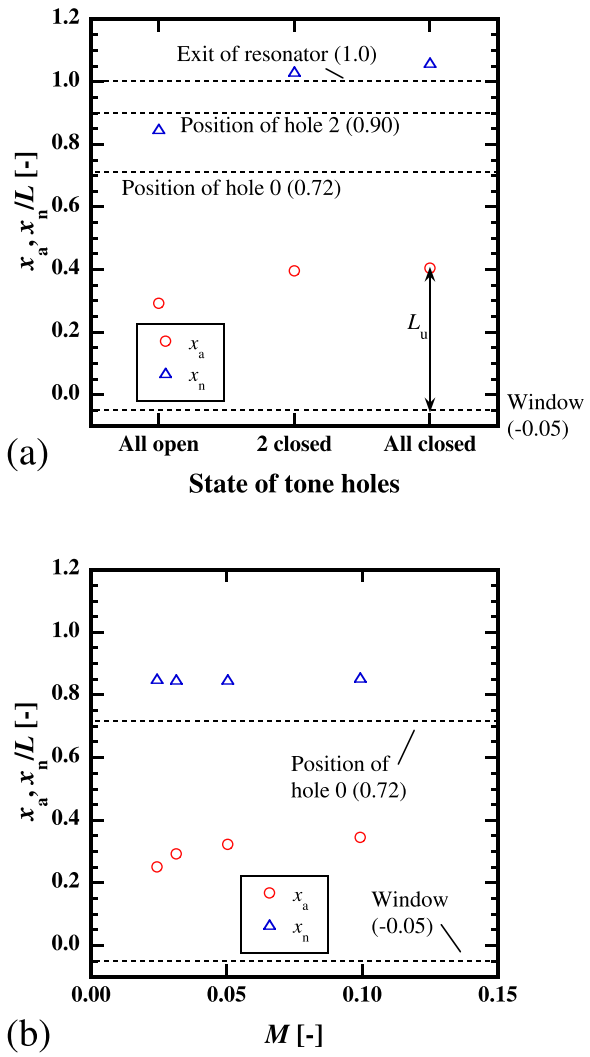

FIG. 18. (Color online) Variation of positions of pressure node, x_n, and anti-node, x_a. (a) Variation in accordance with the state of tone holes at $M = 0.031$. (b) Variation in accordance with Mach number in the case all tone holes are open.

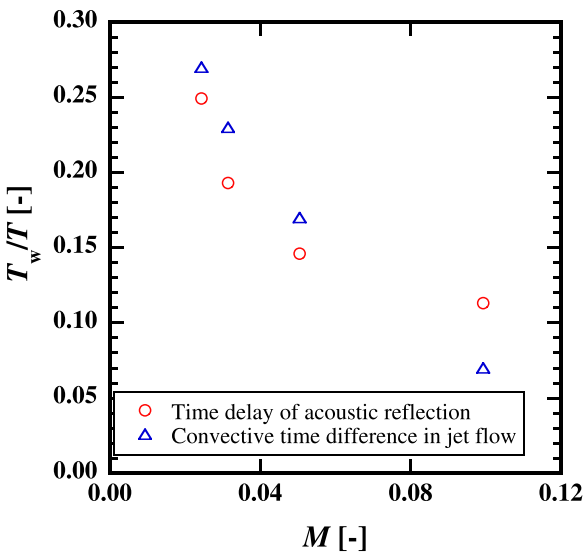

FIG. 19. (Color online) Variations of time delay of acoustic reflection occurring around the window estimated by using the position of the anti-node in the resonator (circles) and the convective time difference between the generation of disturbances due to acoustic feedback and the deflection of jet (triangles) due to increasing Mach number.

V. CONCLUSIONS

To clarify the effects of the state of tone holes and Mach number of jet velocity on fluid–acoustic interactions in an actual recorder, flow and acoustic fields were measured and directly simulated on the basis of the compressible Navier-Stokes equations.

The predicted flow fields clarified the mechanism by which self-sustained oscillations (including fluid–acoustic interactions) are maintained. The disturbances in the jet are induced by increasing acoustic particle velocity, convected and intensified downstream, and thereby deflect the jet. These downward and upward deflections generate compression and expansion in the resonator, respectively. This mechanism of acoustic radiation is consistent with the jet-drive model, where the pressure fluctuations due to the deflection induce a dipolar acoustic field around the edge.

Also, it was clarified that fine two-dimensional vortices become apparent in the jet and intensify the sound pressure levels at higher harmonic frequencies at high Mach number ($M = 0.099$), where the change from the first mode to the second one occurs.

According to the predicted acoustic fields in the resonator, the standing wave is formed in the region between the window and the resonator exit in the case that all holes are closed, while it is formed in the region between the window and the open tone hole closest to the window in the case that one or more holes are open. Also, the effects of the state of tone holes and the Mach number on the positions of anti-nodes and nodes of pressure were identified. The time delay of the acoustic reflection around the window was computed and compared with the convective time difference between the generation of the disturbances and the most intense deflection in the jet flow.

ACKNOWLEDGMENTS

The present study was supported by JSPS KAKENHI Grant No. 26 820 044 and through the Next-generation Supercomputer Strategy Program by the Ministry of Education, Culture, Sports, Science, and Technology of Japan (MEXT).

[1]B. Fabre, J. Gilbert, A. Hirschberg, and X. Pelorson, "Aeroacoustics of musical instruments," Annu. Rev. Fluid Mech. **44**, 1–25 (2012).
[2]H. von Helmholtz, *On the Sensation of Tones*, translated by A. J. Ellis (Dover, New York, 1954), pp. 88–94.
[3]Lord Rayleigh (J. W. Strutt), *The Theory of Sound* (Dover, New York, 1945), Vol. 2, Chap. 21.
[4]J. W. Coltman, "Jet drive mechanism in edge tones and organ pipes," J. Acoust. Soc. Am. **60**, 725–733 (1976).
[5]M. P. Verge, R. Causse, B. Fabre, A. Hirschberg, A. P. J. Wijnands, and A. van Steenbergen, "Jet oscillations and jet drive in recorder-like instruments," Acustica **2**, 403–419 (1994).
[6]M. P. Verge, B. Fabre, A. Hirschberg, and A. P. J. Wijnands, "Sound production in recorder-like instrument. I. Dimensionless amplitude of the internal acoustic field," J. Acoust. Soc. Am. **101**, 2914–2924 (1997).
[7]M. P. Verge, A. Hirschberg, and R. Causse, "Sound production in recorderlike instruments. II. A simulation model," J. Acoust. Soc. Am. **101**(5), 2925–2939 (1997).
[8]B. Fabre and A. Hirscherg, "Physical modeling of flue instruments: A review of lumped models," Acust. Acta Acust. **86**(4), 599–610 (2000).
[9]M. Meissner, "Aerodynamically excited acoustic oscillations in cavity resonator exposed to an air jet," Acust. Acta Acust. **88**, 170–180 (2002).
[10]S. Dequand, J. F. H. Willems, M. Leroux, R. Vullings, M. van Weert, C. Thieulot, and A. Hirschberg, "Simplified models of the instruments: Influence of mouth geometry on the sound source," J. Acoust. Soc. Am. **113**(3), 1724–1735 (2003).
[11]J. W. Coltman, "Momentum transfer in jet excitation of flute-like instruments," J. Acoust. Soc. Am. **69**(4), 1164–1168 (1981).
[12]A. Powell, "Theory of vortex sound," J. Acoust. Soc. Am. **36**, 177–195 (1964).
[13]M. S. Howe, "Contributions to the theory of aerodynamic sound with application to excess jet noise and the theory of the flue," J. Fluid Mech. **71**, 625–673 (1975).
[14]B. Fabre, A. Hirschberg, and A. P. J. Wijnands, "Vortex shedding in steady oscillation of a flue organ pipe," Acust. Acta Acust. **82**, 863–877 (1996).
[15]S. Yoshikawa, H. Tashiro, and Y. Sakamoto, "Experimental examination of vortex-sound generation in an organ pipe: A proposal of jet vortex-layer formation model," J. Sound Vib. **331**, 2558–2577 (2012).
[16]L. Cremer and H. Ising, "Die selbsterregten Schwingungen von Orgelpfeifen" ("The self-sustained vibrations of organ pipes"), Acustica **19**(3), 143–153 (1967).
[17]N. H. Fletcher, "Sound production by organ flue pipes," J. Acoust. Soc. Am **60**(4), 926–936 (1976).
[18]S. Yoshikawa and J. Saneyoshi, "Feedback excitation mechanism in organ pipes," J. Acoust. Soc. Jpn. (E) **1**, 175–191 (1980).
[19]J. W. Coltman, "Jet behavior in the flute," J. Acoust. Soc. Am. **92**(1), 74–83 (1992).
[20]A. H. Benade, "Measured end corrections for woodwind tone holes," J. Acoust. Soc. Am. **41**, 1609 (1967).
[21]D. H. Keefe, "Theory of the single woodwind tone hole," J. Acoust. Soc. Am. **72**(3), 676–687 (1982).
[22]J.-P. Dalmont, C. J. Nederveen, and N. Joly, "Radiation Impedance of tubes with different flanges: Numerical and experimental investigations," J. Sound Vib. **244**(3), 505–534 (2001).
[23]C. Segoufin, B. Fabre, M. P. Verge, A. Hirschberg, and A. P. J. Wijnands, "Experimental study of the influence of the mouth geometry on sound production in a recorder-like instrument: Windway length and chamfers," Acust. Acta Acust. **86**, 649–661 (2000).
[24]R. Auvray, B. Fabre, and P. Kagree, "Regime change and oscillation thresholds in recorder-like instruments," J. Acoust. Soc. Am. **131**(2), 1574–1585 (2012).
[25]N. Giordano, "Simulation studies of a recorder in three dimensions," J. Acoust. Soc. Am. **135**(2), 906–916 (2014).
[26]N. Bak, "Pitch, temperature and blowing pressure in recorder playing study of treble recorders," Acustica **22**, 296–299 (1969).
[27]M. Miyamoto, Y. Ito, T. Iwasaki, T. Akamura, K. Takahashi, T. Takami, T. Kobayashi, A. Nishida, and M. Aoyagi, "Numerical study on acoustic oscillations of 2D and 3D flue organ pipe like instruments with compressible LES," Acust. Acta Acust. **99**, 154–171 (2013).
[28]S. K. Lele, "Compact finite difference schemes with spectral-like resolution," J. Comput. Phys. **103**, 16–42 (1992).
[29]P. Angot, C. H. Bruneau, and P. Frabrie, "A penalization method to take into account obstacles in viscous flows," Numer. Math. **81**, 497–520 (1999).
[30]Q. Liu and O. V. Vasilyev, "A Brinkman penalization method for compressible flows in complex geometries," J. Comp. Phys. **227**, 946–966 (2007).
[31]R. Mittal and G. Iaccarino, "Immersed boundary methods," Annu. Rev. Fluid Mech. **37**, 239–261 (2005).
[32]D. P. Rizzetta and M. R. Visbal, "Large-Eddy simulation of supersonic cavity flow fields including flow control," AIAA J. **41**, 1452–1462 (2003).
[33]C. Bogey and C. Bailly, "Large eddy simulations of round free jets using explicit filtering with/without dynamic Smagorinsky model," Int. J. Heat Fluid Flow **27**, 603–610 (2006).
[34]K. Matsuura and C. Kato, "Large–eddy simulation of compressible transitional flows in a low-pressure turbine cascade," AIAA J. **45**, 442–457 (2007).
[35]C. Bogey and C. Bailly, "Turbulence and energy budget in a self-preserving round jet: Direct evaluation using large eddy simulation," J. Fluid Mech. **627**, 129–160 (2009).
[36]H. Yokoyama and C. Kato, "Fluid-acoustic interactions in self-sustained oscillations in turbulent cavity flows, I. Fluid-dynamic oscillations," Phys. Fluids **21**, 105103 (2009).
[37]H. Yokoyama, K. Kitamiya, and A. Iida, "Flows around a cascade of flat plates with acoustic resonance," Phys. Fluids **25**(10), 106104 (2013).
[38]D. V. Gaitonde and M. R. Visbal, "Pade-type higher-order boundary filters for the Navier-Stokes equations," AIAA J. **38**, 2103–2112 (2000).
[39]K. W. Thompson, "Time dependent boundary conditions for hyperbolic systems," J. Comput. Phys. **68**, 1–24 (1987).
[40]T. J. Poinsot and S. K. Lele, "Boundary conditions for direct simulations of compressible viscous flows," J. Comput. Phys. **101**, 104–129 (1992).
[41]J. W. Kim and D. J. Lee, "Generalized characteristic boundary conditions for computational aeroacoustics," AIAA J. **38**(11), 2040–2049 (2000).
[42]A. H. Benade, "On woodwind instrument bores," J. Acoust. Soc. Am. **31**(2), 137–146 (1959).
[43]A. H. Benade, "On the mathematical theory of woodwind finger holes," J. Acoust. Soc. Am. **32**(12), 1591–1608 (1960).
[44]J. W. Coltman, "Sounding mechanism of the flute and organ pipe," J. Acoust. Soc. Am. **44**(4), 983–992 (1968).
[45]G. Kooijman, A. Hirschberg, and J. Golliard, "Acoustical response of orifices under grazing flow: Effect of boundary layer profile and edge geometry," J. Sound Vib. **315**, 849–874 (2008).
[46]H. R. Graf and S. Ziada, "Excitation source of a side-branch shear layer," J. Sound Vib. **329**, 2825–2842 (2010).
[47]D. Tonon, A. Hirschberg, J. Golliard, and S. Ziada, "Aeroacoustics of pipe systems with closed branches," Int. J. Aeroacoust. **10**(2–3), 201–276 (2011).